ACS APPLIED MATERIALS & INTERFACES

Research Article

www.acsami.org

High-Flux Graphene Oxide Nanofiltration Membrane Intercalated by Carbon Nanotubes

Yi Han, Yanqiu Jiang, and Chao Gao*

MOE Key Laboratory of Macromolecular Synthesis and Functionalization, Department of Polymer Science and Engineering, Zhejiang University, Hangzhou 310027, China

Supporting Information

ABSTRACT: A sort of novel high-flux nanofiltration membrane was fabricated by synergistic assembling of graphene and multiwalled carbon nanotubes (MWNTs), in which graphene played the role of molecular sieving and MWNTs expanded the interlayer space between neighbored graphene sheets. The MWNT-intercalated graphene nanofiltration membrane (G-CNTm) showed a water flux up to 11.3 L m^{-2} h^{-1} bar^{-1}, more than 2 times that of the neat graphene nanofiltration membrane (GNm), while keeping high dye rejection (>99% for Direct Yellow and >96% Methyl Orange). The G-CNTm also showed good rejection ratio for salt ions (i.e., 83.5% for Na_2SO_4, 51.4% for NaCl). We also explored the antifouling performance of G-CNTm and GNm with bovine serum albumin (BSA), sodium alginate (SA) and humic acid (HA). Both G-CNTm and GNm possessed excellent antifouling performance for SA and HA but inferior for BSA because of the strong interaction between protein and graphene sheets.

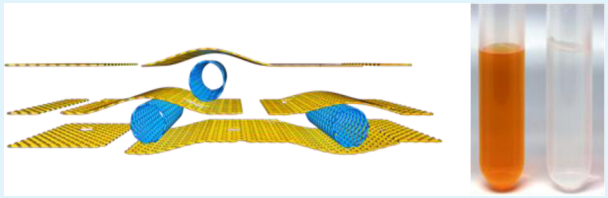

KEYWORDS: *graphene membrane, carbon nanotubes, high-flux, nanofiltration, antifouling*

INTRODUCTION

Graphene is mechanically robust,[1] chemical resistant[2,3] and impermeable to gas and water.[4] As a result, this one-atom-thick two-dimensional (2D) carbon material is a promising candidate for next generation separation nanomaterials by making specified pores on it.[5,6] It also has been proved that graphene membranes (GMs) formed by stacked graphene oxide (GO) or chemically converted graphene (CCG) with aligned 2D nanochannel arrays can efficiently separate molecules in gas or liquid phase.[7−18] Especially, owing to the frictionless and ultrafast water flow inside the well-defined carbon nanochannels, GMs are thought to have great potential in the water treatment field.[11,13,15−17,19−21] GMs can be obtained simply by vacuum filtration or spin coating from GO solution due to the high aspect ratio of GO sheets. The high-speed, low-cost and environmentally benign fabrication processes endow GMs the potential possibility for large-scale production.[2] Because of the strong hydrogen bonds and hydrophobic interaction between GO flakes, these GMs are able to keep the structural integration in air and water surroundings.[12,22]

The mass transportation in GM greatly relies on their microstructure and the feed graphene derivates. The size of the nanochannel formed by adjacent graphene flakes or wrinkled graphene in GMs varies from 1 to 5 nm, leading to a wide range of pure water flux from tens to hundreds L m^{-2} h^{-1} bar^{-1}.[10,11,13,14,17,18] Li's group first prepared GM using CCG by vacuum filtration and explored the potential application in nanofiltration (NF) process which showed pure water flux of 40 L m^{-2} h^{-1} bar^{-1} and rejection ratio of 67% for Direct Yellow (DY).[10] The sub-3 nm corrugation on CCG is thought to be the water transport channels, of which size can be adjusted by the hydrothermal treatment temperature. Similarly, taking advantage of the corrugation on the graphene sheets, Huang et al. reported that GO membrane showed an 85% rejection ratio for Evans blue (EB) with a high water flux of 71 L m^{-2} h^{-1} bar^{-1}.[14] Mi's group applied a layer-by-layer method to deposit GO nanosheets on a porous support and 1,3,5-benzenetricarbonyl trichloride as a cross-linking reagent. They demonstrated that a 15-layered GO membrane showed a 26% rejection for 0.01 M Na_2SO_4 solution with water flux around 25 L m^{-2} h^{-1} bar^{-1}.[13]

Although previously reported GMs showed high pure water flux, the rejection ratios were usually much lower than those of commercial NF membranes, so that they can barely be called NF membranes. We also reported a neat graphene nanofiltration membrane (GNm) made by densely stacked CCG with a comparable rejection ratio to commercial NF membrane (60% for 0.01 M Na_2SO_4 and 99% for dyes), but possessing a limited water flux (3.3 L m^{-2} h^{-1} bar^{-1}).[23] It was hypothesized that the narrow space between graphene sheets in GMs might be the main reason for their low water flux. In the present paper, to further increase the water flux of GNm, we designed a graphene/carbon nanotubes composite membranes (G-CNTm) by assembling refluxed GO (rGO) and multiwalled carbon nanotubes (MWNTs) on a porous substrate, as shown in Figure 1a,b. In this design, we applied MWNTs as a

Received: February 2, 2015
Accepted: April 2, 2015
Published: April 2, 2015

DOI: 10.1021/acsami.5b00986
ACS Appl. Mater. Interfaces 2015, 7, 8147−8155

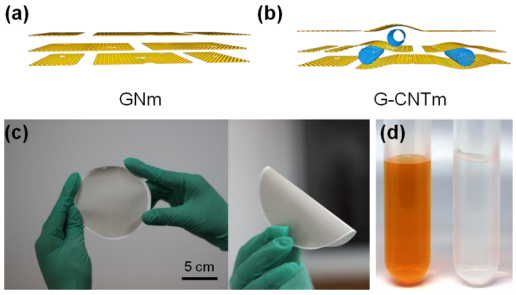

Figure 1. Schematic representation of the structure and water transport path for (a) GNm and (b) G-CNTm. The yellow sheets represent rGO here. (c) Digital photos of a piece of G-CNTm with the diameter of 100 mm. (d) Photographic image shows the color change of 0.05 g L^{-1} MO solution (left) and the collected filtrate (right).

"nanowedge" to expand the interlayer space between neighbored graphene sheets. As expected, the pure water flux of the optimized G-CNTm was more than 2 times that of the GNm counterpart without losing the rejection ratios to organic dye (>99% for Direct Yellow and >96% Methyl Orange). This paper provides a new strategy for the design of high-performance graphene based membranes and also gives us a deep understanding of the real transport and rejecting mechanism of GNm. Additionally, for the first time, the antifouling ability of these graphene base membranes was also investigated and discussed.

EXPERIMENTAL SECTION

Materials. Graphite powder (40 μm) was purchased from Qingdao Henglide Graphite Co., Ltd. MWNTs were purchased from Tsinghua-Nafine Nano-Powder Commercialization Engineering Centre in Beijing (>95% purity). Polyvinylidene fluoride (PVDF) ultrafiltration (UF) membranes with a pore size of 50 nm were provided by the Beijing Hai Cheng Shi Jie CO., Ltd. The AAO disk (Anodisc 47) with a pore size of around 200 nm was purchased from Whatman. Direct Yellow ($C_{16}H_{10}N_2Na_2O_7S_2$) and Methyl Orange ($C_{14}H_{14}N_3SO_3Na$) were provided by Heowns Biochemical Technology CO., Ltd. All the other reagents were purchased from Aldrich and used as received. Milli-Q water was applied in all the testing and preparation processes.

Characterization. X-ray diffraction (XRD) measurement was carried out on X'Pert PRO diffractometer equipped with Cu Kα radiation (40 kV, 40 mA). The morphology of membranes was observed by a Hitachi S4800 field-emission scanning electronic microscopy (SEM) system. Transmission electron microscopy (TEM) images were obtained on a JEOL JEM2010 electron microscope at 200 kV. The surface topology of membranes was examined by an NSK SPI3800 atomic force microscopy (AFM) system, under tapping mode. The mean roughness (Ra) was determined at an area of 4 × 4 μm, from the averages of at least three sections of each membrane. The contact angles of water for the prepared membranes were determined on an optical instrument (OCA20, Dataphysics, Germany) equipped with video capture at 25 °C. The surface charge characterization of the membranes were studied by SurPASS ζ-potential analyzer (Anton Paar, Austria) with a 1 mmol L^{-1} KCl solution circulated through the measuring cell. 0.05 mol L^{-1} HCl and NaOH solutions were used to adjust the pH of the flowing phase in order to monitor the ζ-potential change at different pH values. UV−vis spectra were obtained to determine the concentrations of dye solutions on a Varian Cary 300 Bio UV−vis spectrophotometer. Salt concentrations were measured using electrical conductivity (DDS-307, Shanghai Leici Instrument Co.).

Preparation of rGO and Acid Treated MWNT. Narrow-distributed GO dispersion was synthesized according a modified Hummer's method followed by a centrifugal classification described in the previous work.[23−26] To the flask was added the as-prepared GO aqueous dispersion (50 mL, 0.5 mg mL^{-1}), and the solution was heated to reflux for 2 h. After cooling down to room temperature, the resulting uniform dark black dispersion was centrifuged and washed by pure water for three times, giving the stable rGO dispersion.

Acid treated MWNT was prepared according to ref 27.

Fabrication of G-CNTms. As shown in Table 1, a series of G-CNTms with different MWNT contents were prepared. Taking G-CNTm(8:1) as an example, (the number in the parentheses denotes the mass ratio of rGO to MWNT), an extremely dilute MWNT dispersion was prepared by adding 50 μL of MWNT dispersion (0.5 mg mL^{-1}, 25 μg) into water (300 mL) followed by 30 min of ultrasonication. 400 μL of rGO dispersion (0.5 mg mL^{-1}, 200 μg) was added to this solution, followed by 1 min of ultrasonication. Then the rGO and CNT mixture dispersion was filtrated under vacuum on a PVDF UF membrane with an effective diameter of 100 mm. As a control sample, a GNm without the addition of CNT was prepared by the same method. All the membranes prepared were dried in a vacuum for 24 h at 40 °C, and each membrane was cut into four circular samples with a diameter of 20 mm for the performance tests. Samples for AFM and SEM characterizations were prepared by pasting a piece of sample on the silica substrate.

For the samples for TEM characterization, G-CNTm(2:1) was prepared on AAO porous film by the same method mentioned previously. The skin layer of the G-CNTm(2:1) (assembled by graphene and MWNT) could be exfoliated from the substrate and float on the water surface just by immersing the membrane into water because of the weak interaction between graphene and the surface of anodized aluminum. Then a piece of them was transported onto a TEM copper grid and dried in a vacuum oven overnight at 40 °C before characterization.

NF Performance Evaluation for GNm and G-CNTms. All the NF performance evaluation was carried out in a self-designed dead-end filtration device with magnetic stirring maintained constant at 450 rpm. The trans-membrane pressure (P) was set by nitrogen pressurization of the cell (in the range of 5−9 bar). A new membrane

Table 1. NF Performance of GNm and G-CNTms with Different MWNTs Loadings[a]

		salts				dyes			
		Na_2SO_4[c]	NaCl[c]	$MgSO_4$[c]	$MgCl_2$[c]	DY(957)[d]		MO(327)[e]	
sample	J_0[b]	R%	R%	R%	R%	R%	J_{DY}[b]	R%	J_{MO}[b]
GNm	4.76	95.1	59.0	82.8	31.7	99.8	4.60	98.5	3.82
G-CNTm(8:1)	8.02	80.9	51.4	44.2	15.6	99.9	4.97	98.0	4.61
G-CNTm(4:1)	8.05	81.0	44.8	42.3	14.0	99.8	6.05	96.5	4.67
G-CNTm(8:3)	9.51	83.5	48.1	40.6	18.7	99.9	6.82	96.0	5.93
G-CNTm(2:1)	11.33	81.0	39.7	30.9	9.6	99.8	9.60	96.1	8.69
G-CNTm(8:5)	12.13	71.2	39.6	25.1	9.5	99.6	10.11	92.0	9.54

[a]Under a driven pressure of 5 bar. [b]The unit is L m^{-2} h^{-1} bar^{-1}. [c]The feeding concentration is 0.01 M. [d]The feeding concentration is 0.02 mM. [e]The feeding concentration is 0.05 g L^{-1}.

DOI: 10.1021/acsami.5b00986
ACS Appl. Mater. Interfaces 2015, 7, 8147−8155

sample with effective area 2.27 cm^{-2} (A) sealed by rubber O-ring and glass cement was used in every experiment. The water flux J (L m^{-2} h^{-1} bar^{-1}) was measured by collecting the permeate water (V) through the membrane using an electronic balance (0.01 g) and calculated using the following equation:

$$J = \frac{V}{A \times t \times P}$$

where t is the operation time. The pure water flux (J_0) was recorded after 1 h of filtration when it went steady at 5 bar and neutral pH. After we switched to salt or dye solution, the permeate flux was determined when the retention rate became stable. Retentate and permeate concentrations (C_r and C_p, respectively) were recorded both during and at the end of each run to monitor the evolution of rejection ratios. The rejection ratios can be calculated by the following equation:

$$R = \frac{1 - C_p}{C_r} \times 100\%$$

The rejection ratios of different salts were measured by the sequence of Na_2SO_4, $MgSO_4$, NaCl and $MgCl_2$ at the concentration of 0.01 M. Before we switched to a different feeding solution, the membrane was washed by pure water directly in the filtration cell with stirring at 450 rpm for 30 min followed by filtrating pure water for 1 h to eliminate the effect of the former solute.

The capabilities of separating organic dyes from water were test applying Direct Yellow (DY, 899 Da) and Methyl Orange (MO, 233 Da). First, the rejecting ratio for Na_2SO_4 of a new membrane sample was tested to make sure the membrane is of proper quality. After a pure water wash, the membrane surface was exposed to dye solution (40 mL) for more than 12 h to rule out the adsorption effect by the membrane. Finally, the rejecting ratio for dye solutions was measured by collecting permeated samples three times.

For each group of samples, the tests for NF performance were performed in triplicate to ensure reproducibility.

Fouling Resistance Test For GNm and G-CNTms. To fully characterize the antifouling property of membranes, BSA, SA and HA were selected to represent protein, polysaccharide and natural organic matter, respectively.[28] All the foulant concentration in feed solution was set to 0.9 g L^{-1}. First, the pure water flux (J_0) of a new membrane was measured. Then the tank was fed with 0.9 g L^{-1} of foulant solution. The water flux (J_1) was measured every 20 min for 2 h. After the filtration, the membrane was washed sufficiently by Milli-Q water for 30 min with stirring at 450 rpm. Again the pure water flux was measured (J_2).

RESULTS AND DISCUSSION

Design of G-CNTm. According to the previous analysis, the small interlayer distance between graphene sheets in GNm is the main reason for its low water flux. The space of the 2D nanochannels is held by the oxidation groups on the graphene sheets.[11] Peng's group reported water flux decline when high pressure was applied on GMs, and they contributed the water flux decrease to the shrinkage of the nanochannels under increasing pressure.[29] Additionally, the nanochannel will also shrink at high ion strength because electrolytes screen the negatively charged carboxyl groups and suppress the electrostatic repulsion between graphene sheets.[29] One possible solution to this problem is to intercalate a nanowedge into the graphene sheets to expand and hold the interlayer space of GNm. As shown in Figure 1a,b, we chose MWNTs as the carbonaceous nanowedge to prepare G-CNTm. There are two reasons for us to choose MWNTs. First, as another type of carbon material, MWNTs have excellent compatibility with graphene and the interlayer spacing can be controlled by the diameter of MWNTs precisely.[30] The diameter of the MWNTs used in this paper is around 50 nm. MWNTs can spread through graphene layer and more water molecules are able to enter the 2D nanochannels. The other reason is that all the selective layer of the G-CNTm is composed of carbon material, which is chemically resistant and quite stable at high temperatures.

Fabrication of rGO. Based on our previous report and some newly published works, the reduction degree of rGO is a critical factor for the performance of GNm, because the frictionless flow of water only occurs in the regions of pristine graphene domains.[11,17,19,20,23] The rich oxidation groups of GO membranes prohibit the ultrafast water transport through pristine graphene channels. On the other hand, GNm formed by highly reduced rGO that contains less oxidized functional groups will lead to narrower interlayer space between adjacent graphene flakes and low water flux.[11] Additionally, highly reduced rGO containing less surface charge (mainly provided by carboxyl groups on the edge of GO sheets) leads to lower salt rejection due to the weaker Donnan exclusion.[31−33] To control the reduction to a suitable degree, refluxing, a gentle reaction condition without any reducing agent, was chosen here. After 2 h of refluxing in water, the light brown pristine GO dispersion turned into darker rGO dispersion. The reduction degree of rGO could be monitored by the interlayer space using XRD measurement. GO and fully reduced GO usually show single peak at about 11° and 26°, respectively, in the XRD spectra. Whereas two broadened peaks in the rGO XRD spectrum roughly located at 11° and 26° (as shown in Figure 2a) indicate that GO was partly reduced by heat.[23,34] UV−vis spectra of GO and rGO give more detailed information about reduction (Figure 2b). rGO has stronger absorbance in the broad visible light region 300−700 nm, meaning larger aromatic domains were recovered than that in pristine GO.[35] It is thought that these large conjugated aromatic domains

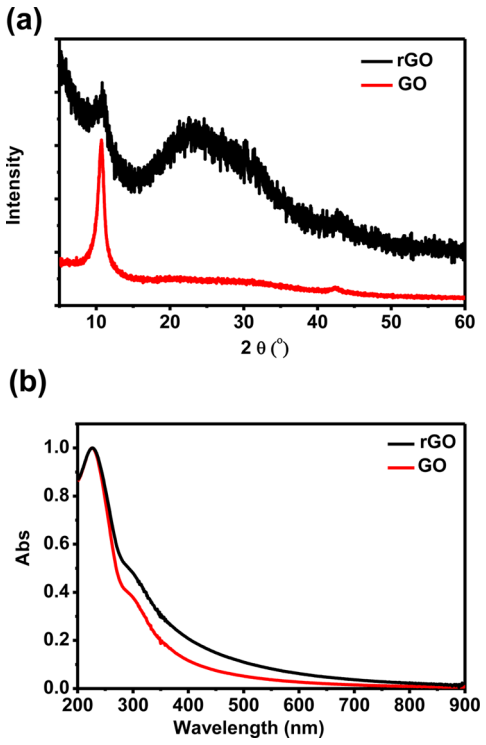

Figure 2. (a) XRD patterns and (b) UV−vis spectra of rGO and pristine GO used in this work.

DOI: 10.1021/acsami.5b00986
ACS Appl. Mater. Interfaces 2015, 7, 8147−8155

provide mechanical strength for the GNm by the force of hydrophobic interaction. The shoulder peak around 300 nm attributed to n−π^* transitions of the carbonyl groups is maintained, which indicates that the carboxyl groups cannot be removed by refluxing.

Fabrication of GNm and G-CNTm. Figure3a shows a typical SEM image of a PVDF UF membrane with a pore size of 50 nm. After deposited by rGO, the pores were uniformly covered by rGO flakes without visible defects (Figure 3b). Akin to the thin-film composite membrane (TFC) design, which is quite common in commercial NF membranes,[36] selective layers of GNm must be defect-free to achieve a desired selectivity. On the other hand, the thickness of the selective layer should be as thin as possible because a thinner selective layer leads to lower hydraulic resistance and shorter diffusive path length for water to transport through the membrane. The thickness of the GNm can be controlled by the amount of graphene loaded on the porous support. We investigate the relationship between rGO loading and membrane performance and the GNm. The GNm with rGO loading of 25.4 mg m^{-2} showed salt rejection of >95% for 0.01 M Na_2SO_4 and water flux of 4.76 L m^{-2} h^{-1} bar^{-1}. GNm with lower rGO loading than 25.4 mg m^{-2} gave unreliable performance because defects (uncoated pores) appeared frequently and GNm with higher rGO loading showed inferior water flux. Given that the area density of graphene is 0.77 mg m^{-2}, the thickness of graphene is 0.34 nm and the interlayer distance between graphene layers in dry state is 0.9 nm, the thickness of GNm with rGO loading of 25.4 mg m^{-2} could be roughly estimated to be 40 nm.[17] Compared with some high-flux commercial NF membrane, the water flux of GNm is relatively low although the thickness is quite small which might be contributed to the narrow nanochannel and relatively longer water transport path caused by the cross-lying construction of capillary network.

As shown in Figure 1c, the ultrathin selective layer of G-CNTm was uniformly assembled on the PVDF support membrane and the composite membrane can be bent randomly without any detectable defects. Figure 3c,d gives more details about the microscopic structure of G-CNTm. MWNTs inserted into graphene sheets without disturbing the morphology of graphene layer of the membrane due to the good flexibility of rGO and the excellent compatibility between graphene and CNTs. From Figure 3d, MWNTs in different layers can be distinguished by the varied darkness of the MWNTs. No obvious aggregation of MWNTs can be found due to the good dispersity in water after acid treatment. We fabricated five different G-CNTms in this paper with the mass ratios of rGO to MWNTs ranging from 8:1 to 8:5, and the rGO loadings of all these membranes were 25.4 mg m^{-2}. The surface morphology of G-CNTm with different MWNTs loadings was characterized by SEM, as shown in Figure 4a−e. The MWNT distribute more densely as the loading increased. It should be noted that G-CNTms with more MWNT loading than that of G-CNTm(8:5) led to a fragile selective layer that could not be sealed well with a silicone sealant. This is probably because too much intercalated MWNTs caused the graphene sheets to pack quite loosely and the strength of the resulting membrane is not strong enough. Figure 4f gives the surface morphology measured by AFM. The selective layer is quite thin that the surface topology is basically determined by the concave and convex of the supporting membrane.

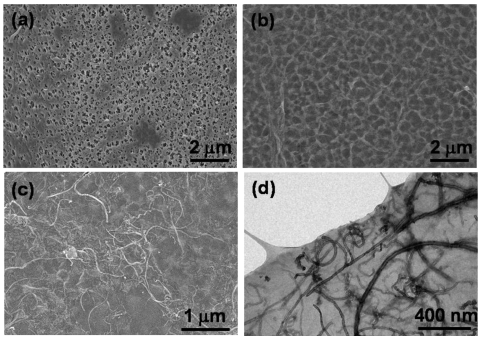

Figure 3. SEM images (top view) of (a) the PVDF supporting membrane with average pore size of 50 nm and (b) GNm. (c) SEM image (top view) of the G-CNTm(2:1). (d) TEM image of a free-standing G-CNTm(2:1) on a copper mesh. The MWNTs were inserted into different layers that could be distinguished by the different contrast of MWNTs.

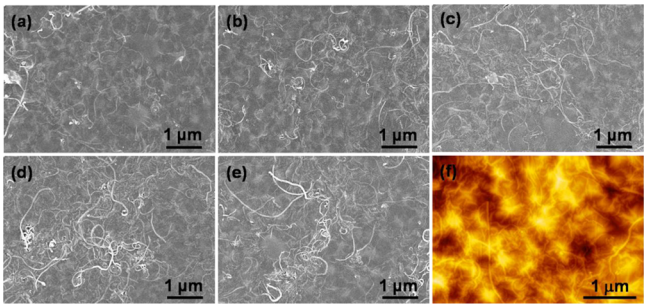

Figure 4. SEM images (top view) of (a) G-CNTm(8:1), (b) G-CNTm(4:1), (c) G-CNTm(8:3), (d) G-CNTm(2:1) and (e) G-CNTm(8:5). (f) AFM image of a G-CNTm(2:1) sample.

NF Performance of G-CNTm. A NF membrane is a type of pressure-driven membrane with a pore size of about 0.5−2.0 nm and a nominal molecular weight cutoff (MWCO, molecular weight of solute that is 90% rejected by the membrane) ranging from 200 to 1000 Da.[37] This separation ability lies between those of nonporous reverse osmosis (RO) membranes and porous UF membranes.[32,38] The pore size of the GNm is decided by the size of the graphene capillaries. As reported in ref 17, the space between the graphene flakes is 1−2 nm in hydrated state, which is in the range of NF membrane. Taking advantage of the low frictional water flow inside the network of 2D nanochannels, GNms were shown to have great potential in NF applications.

We systematically investigated the NF performance of the GNm and G-CNTms. It should be noted that, in this work, we applied a PVDF support membrane with a pore size of 50 nm (200 nm in our previous work),[23] and we found that the smaller pores of the support led to a smoother GNm surface and fewer pin holes or cracks. This improvement increased the rejection ratio for Na_2SO_4 up to 95% without losing the water flux. As shown in Table 1, the salt rejection rate sequence of GNm is R(Na_2SO_4) > R($MgSO_4$) > R(NaCl) > R($MgCl_2$), which shows typical performance of negatively charged NF membrane.[39] The salt rejecting mechanism of charged NF membrane is usually explained by the combination of Donnan exclusion and steric hindrance effect.[32] Thereby, we studied the surface charge of the GNm by ζ-potential tests (Figure 5a) and found that the GNm was highly negatively charged in a wide pH range of 2−10. This agrees with the fact that the carboxyl

DOI: 10.1021/acsami.5b00986
ACS Appl. Mater. Interfaces 2015, 7, 8147−8155

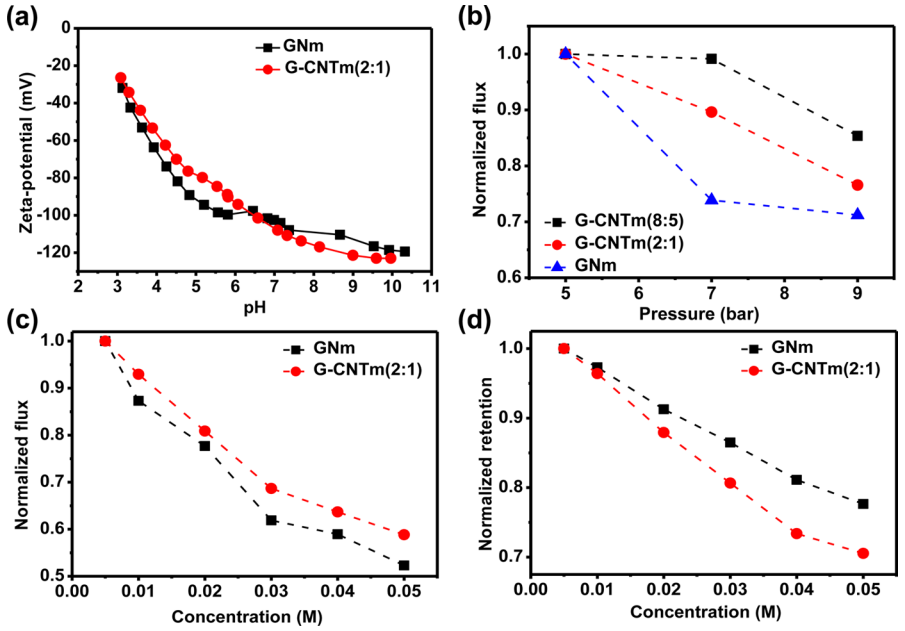

Figure 5. (a) ζ-Potential versus pH curves of GNm and G-CNTm(2:1). (b) Normalized water flux of GNm and G-CNTms under different driven pressures when filtrating DY (0.02 mM). (c) Normalized water flux and (d) normalized rejection ratio of GNm and G-CNTm(2:1) at different salt concentrations when filtrating Na_2SO_4.

groups on the edges of GO were maintained after reflux in water.[31,40] According to the Donnan exclusion theory, as water molecules transport through the membrane driven by the applied pressure, the negative charges on the GNm will repel anions from the membrane and at the same time cations are also retained because of the electroneutrality requirements. This mechanism will result in a high rejection for salts with multivalent anion and monovalentcation.[33,41] Thus, GNm is predicted to have the highest selectivity for Na_2SO_4 and the lowest selectivity for $MgCl_2$, which coincides with the results in Table 1. GNm showed higher rejection for $MgSO_4$ than NaCl because both the hydrated radius values of Mg^{2+} (0.43 nm) and SO_4^{2-} (0.38 nm) are larger than those of Na^+ (0.36 nm) and Cl^- (0.33 nm), indicating that the steric hindrance effect also played an important role in the salt removing ability of GNm.[39] A more than 95% rejection ratio for Na_2SO_4 is the ever reported highest record of GMs to the best of our knowledge, which can be ascribed to the densely and uniformly packed graphene sheets structure.[13,14,29]

The water flux of GNm is relatively low compared with some highly optimized commercial membranes.[42] One of the possible reasons is the small size of the nanochannels. Especially, the interlayer distance of GNm will further decrease when the membrane is filtrating a high concentration salt solution or under high pressure according to refs 20 and 29. On the basis of this assumption, we applied acid treated MWNTs as a nanowedge to increase the size of the nanochannels between graphene sheets. The NF performance of G-CNTms are listed in Table 1, and as expected, the pure water flux (J_0) of G-CNTms increased while the salt rejection rates decreased as more MWNTs were added into the graphene layers. (The water fluxes of GNm and G-CNTm(8:3) at different pH values are shown in Figure S1 of the Supporting Information.) Given that the ζ-potential of the G-CNTms did not change after MWNTs incorporated (Figure 5a), we can attribute the reduction of salt rejection rates to the increase of nanochannel size of G-CNTms. To be specific, for G-CNTm(2:1), the rejection rates for $MgSO_4$ and $MgCl_2$ decreased significantly from 82.8% and 31.7% to 30.9% and 9.6% respectively, but the rejection rates for Na_2SO_4 and NaCl only decreased from 95.1% and 59.0% to 81.0% and 39.7%. This is because the Mg^{2+} has the largest hydrated radius of the four kinds of testing ions. The hydrated radius of Mg^{2+}, Na^+, Cl^- and SO_4^{2-} are 0.43, 0.36, 0.33 and 0.38 nm, respectively.[39] Thereby, the steric hindrance effect played a significantly important role in the retention of $MgSO_4$ and $MgCl_2$. On the contrary, for the smaller ions, steric hindrance effect played a limited role while Donnan exclusion effect was the dominate mechanism. As a result, compared with GNm, the rejection reduction of G-CNTms for Na_2SO_4 and NaCl was much smaller than that for magnesium salts. From the trade-off relation between water flux and solute rejection of G-CNTms, we could deduce that the size of 2D nanocapillary was enlarged by inserting MWNTs into the interlayer space of graphene flakes.

In the organic dye removal tests, according to Table 1, G-CNTm showed great water flux increase without sacrificing the dye rejection. We chose negatively charged DY and MO as target molecules to test the dye removal ability of G-CNTms, whose molecular weights are 957 and 327, respectively, very close to the upper and lower limitations of the NF process. Almost all the G-CNTms showed very high retention rates both for DY (>99.5%) and MO (>96%), except G-CNTm(8:5). Particularly, the G-CNTm(2:1) showed more than twice the water flux of GNm and almost the same rejection rate with GNm. According to the previous analysis, the size of the nanochannels is enlarged by MWNTs, and more water molecules are able to enter the nanochannels in certain time from the edges or pore of the graphene flakes. But the nanochannels are still sufficiently small to block dye molecules resulting in high rejection rates for dyes. The G-CNTm(8:5) showed the highest water flux but also a little lower dye rejection for MO, which indicated that more paths for MO permeation appeared. High pressure or ion strength decreases the interlayer distance leading to even lower water flux

DOI: 10.1021/acsami.5b00986
ACS Appl. Mater. Interfaces 2015, 7, 8147−8155

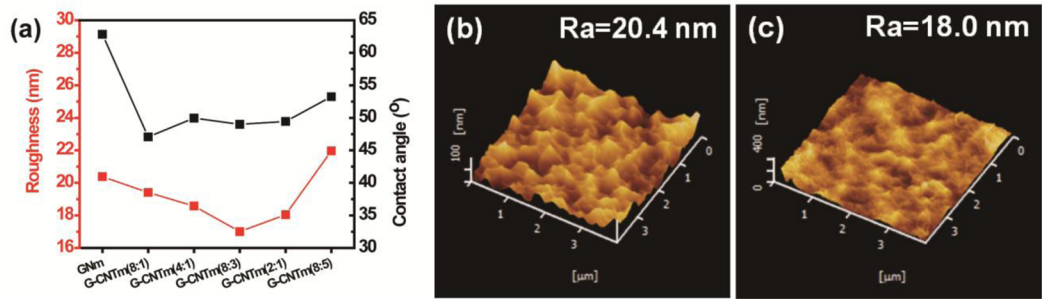

Figure 6. (a) Surface roughness in terms of the average roughness (Ra) and water contact angles of GNm and G-CNTms. Typical surface AFM images and surface roughness analysis for (b) GNm and (c) G-CNTm(2:1).

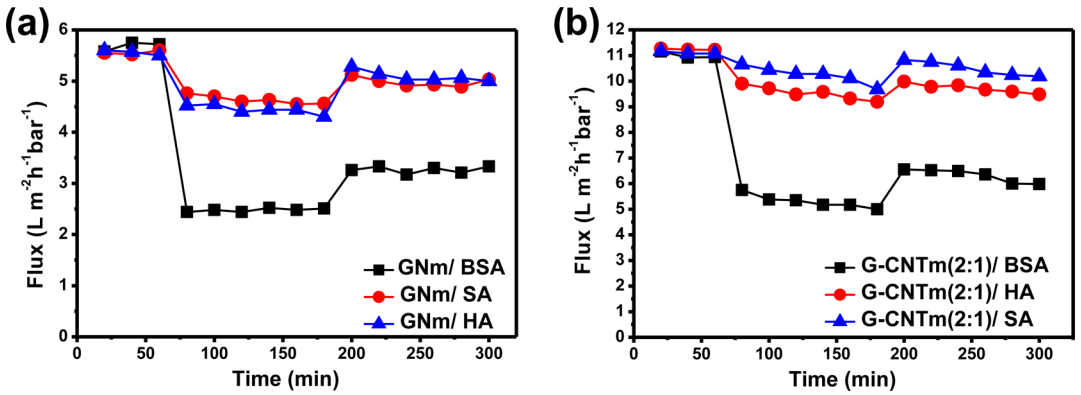

Figure 7. Fouling tests for (a) GNm and (b) G-CNTm(2:1) under 5 bar. Flux was plotted versus time for three periods: pure water flux for 60 min, 0.9 g L^{-1} BSA, HA and SA solution flux for 120 min, and pure water flux after hydraulic washing for 120 min.

according to Peng's report.[29] We tested the water flux of GNm and G-CNTm when filtrating DY under different pressures (as shown in Figure 5b). All the membranes showed water flux decline under higher pressures due to the shrinkage of nanochannels, but the water flux for G-CNTms dropped much slower than that for GNm. DY rejection ratio decline kept invariant in the high pressure tests, which indicated that GNm and G-CNTm were strong enough to sustain high pressure up to 9 bar. Increasing the salt concentration also decreased the water flux of both GNm and G-CNTm(2:1) (as shown in Figure 5c) when filtrating Na_2SO_4. Similarly, the normalized water flux of G-CNTm(2:1) decreased slower than that of GNm as the concentration of Na_2SO_4 increased. On the other hand, the normalized rejection ratio for Na_2SO_4 of G-CNTm(2:1) dropped quicker than that of GNm (Figure 5d). The reason is that the Donnan exclusion effect is the dominate mechanism for G-CNTm(2:1) when filtrating Na_2SO_4, and high concentration electrolytes screen the negative charge on the graphene sheets, which weaken the Donnan exclusion effect.[43] For GNm, although the Donnan exclusion effect was also screened under high ionic strength but steric hindrance effect also played an important role. As a result, the rejection ratio of GNm dropped slower than that of G-CNTm(2:1). All the results above demonstrate that MWNTs are able to hold the space between graphene layers and maintain high water flux under high pressure and high ion strength.

Assembling MWNTs into GNm makes G-CNTms a novel high-flux NF membrane with high rejection ratios to dyes, and this not only provides us a new design idea for adjusting the graphene membranes pore size with nanoadditives but also gives a solid proof for water transport between graphene layers, because if water transport directly through the pores or pin holes on graphene, adding MWNTs in graphene layers would not lead to higher water flux.

Antifouling Property of GNm and G-CNTm. Fouling resistance ability is crucial to NF membrane applications in water treatment. Fouling is usually caused by accumulation of proteins, micro-organisms and inorganic colloids on the membrane surface.[44−46] Severe fouling disfavors the permeation of desired molecules, diminishes the NF performance and ultimately shortens the lifetime of the membranes. It is reported that the antifouling property is mostly influenced by the hydrophilicity and roughness of the membrane surface. That is because most foulants are absorbed on the membrane by hydrophobic interaction. However, a hydrophilic surface can form a water layer, which retards the adsorption of protein and other foulants. And a smooth membrane has less possibility of a fouling agent being stuck than that in a rough surface.[47] Graphene oxide has been applied to prove the antifouling and chlorine resistance properties in several laboratories owing to its hydrophilic nature and chemical resistance, but unfortunately, such investigations on GNms have not been reported.[44,47]

It might be doubted that adding MWNT into GNm will increase the roughness of the membrane and worsen antifouling properties of G-CNTms. In this paper, we studied the surface roughness of all the prepared membrane in term of average roughness (Ra) and water contact angle as a characterization of hydrophilicity which are listed in Figure 6a. Surprisingly, almost all the G-CNTms showed lower roughness compared with GNm. The Ra of the porous PVDF supporting membrane was 27.5 nm. The Ra of GNm decreased to 20.4 nm (Figure 6a), because graphene flakes covered the holes on the supporting layer. According to the AFM images in

DOI: 10.1021/acsami.5b00986
ACS Appl. Mater. Interfaces 2015, 7, 8147−8155

Figures 4f, and 6b,c, most MWNTs were located at the valley of the supporting membrane and further decreased height difference of the G-CNTms leading to a smaller Ra (as low as 17.0 nm for G-CNTm(8:3)). G-CNTm(8:5) showed little higher roughness than that of GNm, indicating that too many MWNTs would destroy the flattened surface morphology. The roughness of the G-CNTms is much lower than the most common commercial PA NF membrane prepared by interfacial polymerization (170 ± 30 nm) because the reaction degree and rate of interfacial polymerization is very difficult to control.[48] Additionally, G-CNTms were more hydrophilic than GNm, which was demonstrated by the smaller contact angles of water on the G-CNTm, as shown in Figure 6a. Based on the former analysis, G-CNTms were expected to possess better antifouling property than GNm.

We investigated the antifouling performance of both GNm and G-CNTms using 0.9 g/L BSA, SA and HA solution as foulant simulator. Three periods of water flux were recorded in Figure 7: the pure water flux (J_0) before foulant solution was fed, the water flux when filtrating foulant solution (J_1) and the water flux after foulant filtration (J_2). The water flux went through a sharp decline after foulant solution was fed into the tank. After filtration of foulant, the membrane surface was directly washed by deionized water and water flux showed a certain extent of recovery. Generally, the antifouling ability of the membranes is measured in terms of flux recovery ratio (FRR) using following equation:[28]

$$\mathrm{FRR} = \frac{J_2}{J_0} \times 100\%$$

A higher FRR value means the membrane is easier to recovery by hydraulic cleaning. It can be seen from Figure 7 that both GNm and G-CNTm(2:1) show good antifouling performances when the foulant is HA and SA. The FRR values of GNm are 89.6% and 91.5% for SA and HA. And the FRR values of G-CNTm(2:1) reach 94.4% and 86.5% for SA and HA, respectively. Whereas the FRR values of both GNm and G-CNTm(2:1) when filtrating BSA solution are around 57%, which are much lower.

In more details, the fouling process can be analyzed by calculating total fouling ratio (R_t), reversible fouling ratio (R_r) and irreversible fouling ratio (R_{ir}) (Figure 8) using the following equations:[47]

$$R_t = \frac{J_0 - J_1}{J_0} \times 100\%$$

$$R_r = \frac{J_2 - J_1}{J_0} \times 100\%$$

$$R_{ir} = \frac{J_0 - J_2}{J_0} \times 100\% = R_t - R_r$$

As demonstrated in Figure 8, G-CNTm(2:1) shows a lower R_t than GNm for SA and HA, which are all lower than 20%, and this result is in accordance with the roughness and water contact angle analysis. GNm shows a higher R_t (56.4%) and reversible fouling ratio (13.9%) than G-CNTm(2:1) (51.8% and 9.3%, respectively) when filtrating BSA solution, which can also be explained by the higher roughness and lower hydrophilicity of GNm. But different from the case of SA and HA, the irreversible fouling contributes most to the total

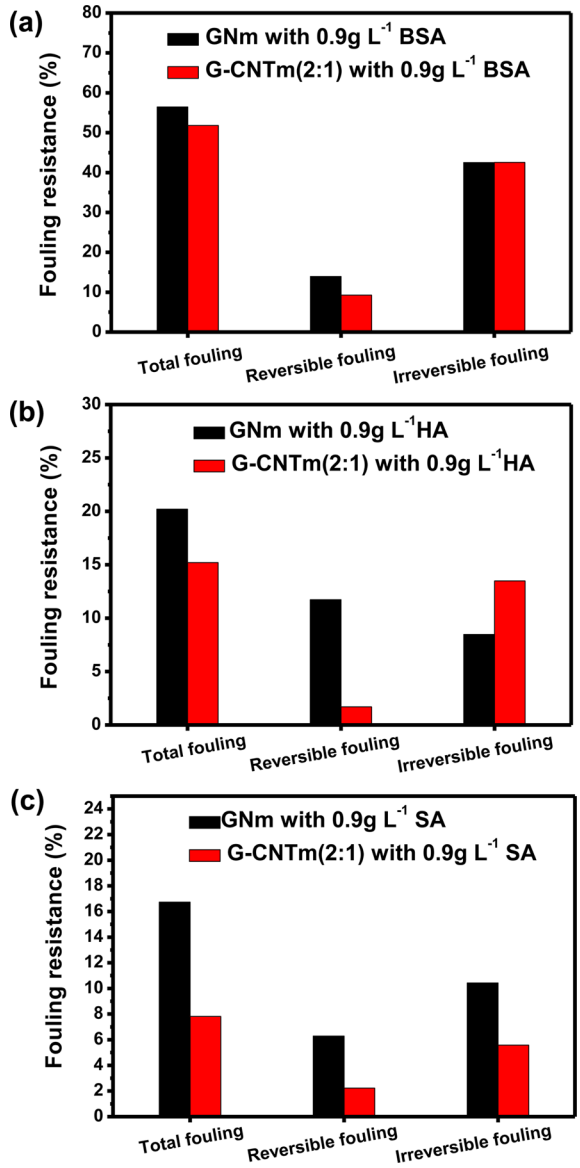

Figure 8. Fouling resistance ratios of GNm and G-CNTm(2:1) for (a) BSA, (b) HA and (c) SA.

fouling of both membranes when filtrating BSA. Knowing that the molecular size of the foulants is much larger than that of nanocapillary of the graphene membrane, the irreversible fouling could not be caused by foulants that stuck into the membrane pores.[49] Given that there are a lot of oxidation groups on the rGO sheets, the possible reason for the high R_{ir} value in the BSA antifouling test might be that protein molecules have strong interactions with the rGO sheets surface, such as hydrogen bonds and static electricity attraction.[50,51] In fact, many research groups have taken advantage of the strong attraction between protein and graphene to fabricate advanced protein detectors or sensors.[50,51] Additionally, the membrane could not be washed efficiently in a dead-end filtration device compared with cross-flow filtration equipment.

It might be doubted that a graphene based membrane without cross-linking is not stable enough in flowing water.[13] In fact, based on our observation, although special care during operation is needed, graphene based membranes in our experiments are strong enough to sustain hydraulic cleaning directly on the membrane surface and even high speed cross

DOI: 10.1021/acsami.5b00986
ACS Appl. Mater. Interfaces 2015, 7, 8147−8155

water flow in the ζ-potential test without detectable membrane damage.

CONCLUSIONS

As a summary, we assembled rGO and acid treated MWNTs to fabricate a novel graphene based high-water-flux NF membrane. Morphology studies demonstrated that uniform dispersity of MWNTs in the 2D nanochannels results in enlarged 2D nanochannels network for fast water transport. NF performance testing showed that G-CNTms with proper amount of MWNTs loadings can increase the water flux by more than 100% and maintain high dye rejection ratios for DY (>99%) and MO (>96%). MWNTs act as space holders between graphene layers and avoid shrinkage of nanochannels at high driven pressure or high ion strength, endowing G-CNTms better NF performance compared with neat GNm. The NF performance of G-CNTm is also competitive among some highly optimized commercial high-flux NF membranes.

For the first time, we preliminarily discussed the antifouling property of a graphene based NF membrane, as graphene was expected to have hopeful potential in these applications. G-CNTms showed a better antifouling ability than GNm due to lower roughness and better hydrophilicity. Compared with a traditional polymeric NF membrane, GNm and G-CNTm performed well in SA and HA antifouling tests as expected, but their antifouling performance for BSA was still under the expectation because of the strong attraction between protein and graphene sheets. Further work, both experimental and theoretical, is urgently required to gain more understanding about the mechanism of fouling graphene based NF membranes. It can be expected that, by carefully and smartly designing the nanostructure, the graphene based membrane is poised to become the next generation NF membrane with extraordinary filtration performance and long-lasting operating lifetime.

ASSOCIATED CONTENT

Supporting Information

Pure water fluxes of GNm and G-CNTm(8:3) at different pH values. This material is available free of charge via the Internet at http://pubs.acs.org.

AUTHOR INFORMATION

Corresponding Author

*C. Gao. E-mail: chaogao@zju.edu.cn. Tel: +86-(0)571-87952088.

Notes

The authors declare no competing financial interest.

ACKNOWLEDGMENTS

This work is supported by the National Natural Science Foundation of China (No. 21325417 and No. 51173162) and Fundamental Research Funds for the Central Universities (No. 2013XZZX003).

REFERENCES

(1) Lee, C.; Wei, X.; Kysar, J. W.; Hone, J. Measurement of the Elastic Properties and Intrinsic Strength of Monolayer Graphene. *Science* **2008**, *321*, 385−388.

(2) Dikin, D. A.; Stankovich, S.; Zimney, E. J.; Piner, R. D.; Dommett, G. H. B.; Evmenenko, G.; Nguyen, S. T.; Ruoff, R. S. Preparation and Characterization of Graphene Oxide Paper. *Nature* **2007**, *448*, 457−460.

(3) Chen, S.; Brown, L.; Levendorf, M.; Cai, W.; Ju, S. Y.; Edgeworth, J.; Li, X.; Magnuson, C. W.; Velamakanni, A.; Piner, R. D.; Kang, J.; Park, J.; Ruoff, R. S. Oxidation Resistance of Graphene-Coated Cu and Cu/Ni Alloy. *ACS Nano* **2011**, *5*, 1321−1327.

(4) Bunch, J. S.; Verbridge, S. S.; Alden, J. S.; van der Zande, A. M.; Parpia, J. M.; Craighead, H. G.; McEuen, P. L. Impermeable Atomic Membranes from Graphene Sheets. *Nano Lett.* **2008**, *8*, 2458−2462.

(5) Koenig, S. P.; Wang, L.; Pellegrino, J.; Bunch, J. S. Selective Molecular Sieving through Porous Graphene. *Nat. Nanotechnol.* **2012**, *7*, 728−732.

(6) O'Hern, S. C.; Stewart, C. A.; Boutilier, M. S. H.; Idrobo, J. C.; Bhaviripudi, S.; Das, S. K.; Kong, J.; Laoui, T.; Atieh, M.; Karnik, R. Selective Molecular Transport through Intrinsic Defects in a Single Layer of CVD Graphene. *ACS Nano* **2012**, *6*, 10130−10138.

(7) Hu, M.; Mi, B. Layer-by-Layer Assembly of Graphene Oxide Membranes via Electrostatic Interaction. *J. Membr. Sci.* **2014**, *469*, 80−87.

(8) Mi, B. Graphene Oxide Membranes for Ionic and Molecular Sieving. *Science* **2014**, *343*, 740−742.

(9) Ying, Y.; Sun, L.; Wang, Q.; Fan, Z.; Peng, X. In-Plane Mesoporous Graphene Oxide Nanosheet Assembled Membranes for Molecular Separation. *RSC Adv.* **2014**, *4*, 21425−21428.

(10) Qiu, L.; Zhang, X. H.; Yang, W. R.; Wang, Y. F.; Simon, G. P.; Li, D. Controllable Corrugation of Chemically Converted Graphene Sheets in Water and Potential Application for Nanofiltration. *Chem. Commun.* **2011**, *47*, 5810−5812.

(11) Nair, R. R.; Wu, H. A.; Jayaram, P. N.; Grigorieva, I. V.; Geim, A. K. Unimpeded Permeation of Water through Helium-Leak-Tight Graphene-based Membranes. *Science* **2012**, *335*, 442−444.

(12) Sun, P.; Zhu, M.; Wang, K.; Zhong, M.; Wei, J.; Wu, D.; Xu, Z.; Zhu, H. Selective Ion Penetration of Graphene Oxide Membranes. *ACS Nano* **2013**, *7*, 428−437.

(13) Hu, M.; Mi, B. Enabling Graphene Oxide Nanosheets as Water Separation Membranes. *Environ. Sci. Technol.* **2013**, *47*, 3715−3723.

(14) Huang, H.; Song, Z.; Wei, N.; Shi, L.; Mao, Y.; Ying, Y.; Sun, L.; Xu, Z.; Peng, X. Ultrafast Viscous Water Flow through Nanostrand-Channelled Graphene Oxide Membranes. *Nat. Commun.* **2013**, *4*, 2979.

(15) Kim, H. W.; Yoon, H. W.; Yoon, S. M.; Yoo, B. M.; Ahn, B. K.; Cho, Y. H.; Shin, H. J.; Yang, H.; Paik, U.; Kwon, S.; Choi, J. Y.; Park, H. B. Selective Gas Transport through Few-Layered Graphene and Graphene Oxide Membranes. *Science* **2013**, *342*, 91−95.

(16) Li, H.; Song, Z.; Zhang, X.; Huang, Y.; Li, S.; Mao, Y.; Ploehn, H. J.; Bao, Y.; Yu, M. Ultrathin, Molecular-Sieving Graphene Oxide Membranes for Selective Hydrogen Separation. *Science* **2013**, *342*, 95−98.

(17) Joshi, R. K.; Carbone, P.; Wang, F. C.; Kravets, V. G.; Su, Y.; Grigorieva, I. V.; Wu, H. A.; Geim, A. K.; Nair, R. R. Precise and Ultrafast Molecular Sieving through Graphene Oxide Membranes. *Science* **2014**, *343*, 752−754.

(18) Tang, Y. P.; Paul, D. R.; Chung, T. S. Free-Standing Graphene Oxide Thin Films Assembled by a Pressurized Ultrafiltration Method for Dehydration of Ethanol. *J. Membr. Sci.* **2014**, *458*, 199−208.

(19) Wei, N.; Peng, X.; Xu, Z. Understanding Water Permeation in Graphene Oxide Membranes. *ACS Appl. Mater. Interfaces* **2014**, *6*, 5877−5883.

(20) Boukhvalov, D. W.; Katsnelson, M. I.; Son, Y. W. Origin of Anomalous Water Permeation through Graphene Oxide Membrane. *Nano Lett.* **2013**, *13*, 3930−3935.

(21) Kannam, S. K.; Todd, B. D.; Hansen, J. S.; Daivis, P. J. Slip Length of Water on Graphene: Limitations of Non-equilibrium Molecular Dynamics Simulations. *J. Chem. Phys.* **2012**, *136*, 024705.

(22) Xu, Z.; Gao, C. Graphene in Macroscopic Order: Liquid Crystals and Wet-Spun Fibers. *Acc. Chem. Res.* **2014**, *47*, 1267−1276.

(23) Han, Y.; Xu, Z.; Gao, C. Ultrathin Graphene Nanofiltration Membrane for Water Purification. *Adv. Funct. Mater.* **2013**, *23*, 3693−3700.

DOI: 10.1021/acsami.5b00986
ACS Appl. Mater. Interfaces 2015, 7, 8147−8155

(24) He, H. K.; Gao, C. General Approach to Individually Dispersed, Highly Soluble, and Conductive Graphene Nanosheets Functionalized by Nitrene Chemistry. *Chem. Mater.* **2010**, *22*, 5054−5064.
(25) Xu, Z.; Gao, C. *In Situ* Polymerization Approach to Graphene-Reinforced Nylon-6 Composites. *Macromolecules* **2010**, *43*, 6716−6723.
(26) Xu, Z.; Gao, C. Graphene Chiral Liquid Crystals and Macroscopic Assembled Fibres. *Nat. Commun.* **2011**, *2*, 571.
(27) Gao, C.; Vo, C. D.; Jin, Y. Z.; Li, W. W.; Armes, S. P. Multihydroxy Polymer-Functionalized Carbon Nanotubes: Synthesis, Derivatization, and Metal Loading. *Macromolecules* **2005**, *38*, 8634−8648.
(28) Zhang, Y.; Su, Y.; Peng, J.; Zhao, X.; Liu, J.; Zhao, J.; Jiang, Z. Composite Nanofiltration Membranes Prepared by Interfacial Polymerization with Natural Material Tannic Acid and Trimesoyl Chloride. *J. Membr. Sci.* **2013**, *429*, 235−242.
(29) Huang, H.; Mao, Y.; Ying, Y.; Liu, Y.; Sun, L.; Peng, X. Salt Concentration, pH and Pressure Controlled Separation of Small Molecules through Lamellar Graphene Oxide Membranes. *Chem. Commun.* **2013**, *49*, 5963−5965.
(30) Sun, H.; Xu, Z.; Gao, C. Multifunctional, Ultra-Flyweight, Synergistically Assembled Carbon Aerogels. *Adv. Mater.* **2013**, *25*, 2554−2560.
(31) Dreyer, D. R.; Park, S.; Bielawski, C. W.; Ruoff, R. S. The Chemistry of Graphene Oxide. *Chem. Soc. Rev.* **2010**, *39*, 228−240.
(32) Hilal, N.; Al-Zoubi, H.; Darwish, N. A.; Mohammad, A. W.; Arabi Abu, M. A Comprehensive Review of Nanofiltration Membranes: Treatment, Pretreatment, Modelling, and Atomic Force Microscopy. *Desalination* **2004**, *170*, 281−308.
(33) Peeters, J. M. M.; Boom, J. P.; Mulder, M. H. V.; Strathmann, H. Retention Measurements of Nanofiltration Membranes with Electrolyte Solutions. *J. Membr. Sci.* **1998**, *145*, 199−209.
(34) Jeong, H. K.; Lee, Y. P.; Jin, M. H.; Kim, E. S.; Bae, J. J.; Lee, Y. H. Thermal Stability of Graphite Oxide. *Chem. Phys. Lett.* **2009**, *470*, 255−258.
(35) Dimiev, A.; Kosynkin, D. V.; Alemany, L. B.; Chaguine, P.; Tour, J. M. Pristine Graphite Oxide. *J. Am. Chem. Soc.* **2012**, *134*, 2815−2822.
(36) Pendergast, M. M.; Hoek, E. M. V. A Review of Water Treatment Membrane Nanotechnologies. *Energy Environ. Sci.* **2011**, *4*, 1946−1971.
(37) Sun, S. P.; Hatton, T. A.; Chan, S. Y.; Chung, T. S. Novel Thin-Film Composite Nanofiltration Hollow Fiber Membranes with Double Repulsion for Effective Removal of Emerging Organic Matters from Water. *J. Membr. Sci.* **2012**, *401*, 152−162.
(38) Bowen, W. R.; Welfoot, J. S. Modelling the Performance of Membrane Nanofiltration: Critical Assessment and Model Development. *Chem. Eng. Sci.* **2002**, *57*, 1121−1137.
(39) Schaep, J.; Van der Bruggen, B.; Vandecasteele, C.; Wilms, D. Influence of Ion Size and Charge in Nanofiltration. *Sep. Purif. Technol.* **1998**, *14*, 155−162.
(40) Erickson, K.; Erni, R.; Lee, Z.; Alem, N.; Gannett, W.; Zettl, A. Determination of the Local Chemical Structure of Graphene Oxide and Reduced Graphene Oxide. *Adv. Mater.* **2010**, *22*, 4467−4472.
(41) Fornasiero, F.; Park, H. G.; Holt, J. K.; Stadermann, M.; Grigoropoulos, C. P.; Noy, A.; Bakajin, O. Ion Exclusion by Sub-2-nm Carbon Nanotube Pores. *Proc. Natl. Acad. Sci. U. S. A.* **2008**, *105*, 17250−17255.
(42) Wu, H.; Tang, B.; Wu, P. Preparation and Characterization of Anti-fouling β-Cyclodextrin/Polyester Thin Film Nanofiltration Composite Membrane. *J. Membr. Sci.* **2013**, *428*, 301−308.
(43) Wang, X. L.; Tsuru, T.; Nakao, S.; Kimura, S. The Electrostatic and Steric-Hindrance Model for the Transport of Charged Solutes through Nanofiltration Membranes. *J. Membr. Sci.* **1997**, *135*, 19−32.
(44) Choi, W.; Choi, J.; Bang, J.; Lee, J. H. Layer-by-Layer Assembly of Graphene Oxide Nanosheets on Polyamide Membranes for Durable Reverse-Osmosis Applications. *ACS Appl. Mater. Interfaces* **2013**, *5*, 12510−12519.
(45) Elimelech, M.; Phillip, W. A. The Future of Seawater Desalination: Energy, Technology, and the Environment. *Science* **2011**, *333*, 712−717.
(46) Nystrom, M.; Kaipia, L.; Luque, S. Fouling and Retention of Nanofiltration Membranes. *J. Membr. Sci.* **1995**, *98*, 249−262.
(47) Zinadini, S.; Zinatizadeh, A. A.; Rahimi, M.; Vatanpour, V.; Zangeneh, H. Preparation of a Novel Antifouling Mixed Matrix PES Membrane by Embedding Graphene Oxide Nanoplates. *J. Membr. Sci.* **2014**, *453*, 292−301.
(48) Johnson, P. M.; Yoon, J.; Kelly, J. Y.; Howarter, J. A.; Stafford, C. M. Molecular Layer-by-Layer Deposition of Highly Crosslinked Polyamide Films. *J. Polym. Sci., Part B: Polym. Phys.* **2012**, *50*, 168−173.
(49) Wright, A. K.; Thompson, M. R. Hydrodynamic Structure of Bovine Serum-Albumin Determined by Transient Electric Birefringence. *Biophys. J.* **1975**, *15*, 137−141.
(50) Tang, L. A. L.; Wang, J.; Loh, K. P. Graphene-based SELDI Probe with Ultrahigh Extraction and Sensitivity for DNA Oligomer. *J. Am. Chem. Soc.* **2010**, *132*, 10976−10977.
(51) Liu, Q.; Shi, J.; Cheng, M.; Li, G.; Cao, D.; Jiang, G. Preparation of Graphene-Encapsulated Magnetic Microspheres for Protein/Peptide Enrichment and MALDI-TOF MS Analysis. *Chem. Commun.* **2012**, *48*, 1874−1876.

DOI: 10.1021/acsami.5b00986
ACS Appl. Mater. Interfaces 2015, 7, 8147−8155